Applied Surface Science 516 (2020) 146115

Contents lists available at ScienceDirect

Applied Surface Science

journal homepage: www.elsevier.com/locate/apsusc

Full Length Article

Tailored electrochemical behavior of ta-C film by glancing angle deposition

Jing Wei[a,b], Peng Guo[a], Linlin Liu[a], Hanchao Li[a,d], Hao Li[a], Shuyuan Wang[a,b], Peiling Ke[a,b], Aiying Wang[a,b,c,*]

[a] Key Laboratory of Marine Materials and Related Technologies, Zhejiang Key Laboratory of Marine Materials and Protective Technologies, Ningbo Institute of Materials Technology and Engineering, Chinese Academy of Sciences, Ningbo 315201, China
[b] Center of Materials Science and Optoelectronics Engineering, University of Chinese Academy of Sciences, Beijing 100049, China
[c] Ningbo Institute of Industrial Technology, Chinese Academy of Sciences, Ningbo 315201, China
[d] School of Physical Science and Technology, Shanghai Tech University, Shanghai 201210, China

ARTICLE INFO

Keywords:
Glancing angle deposition
ta-C
Microstructure
Electrochemical corrosion

ABSTRACT

Tetrahedral amorphous carbon (ta-C) films were obliquely deposited on silicon substrate using a custom-made 45 degree double-bent filtered cathodic vacuum arc (FCVA) system. The effect of glancing angle in a range of 0° to 75° on the growth characteristics, mechanical and electrochemical corrosion behavior of the films were focused. Results showed that increasing the incident angle of carbon ions resulted in a rough surface with agglomerated particles. As the glancing angle changed from 0° to 75°, the residual stress of ta-C film decreased by 28.8%, while the high hardness exceeding 30 GPa were maintained in the films due to the small reduction (13.6%) of sp^3 hybridized carbon content. The electrochemical corrosion tests in 3.5 wt% NaCl solution revealed that the superior corrosion resistances were obtained at glancing angle of 45°, which could be discussed in terms of the relatively high sp^3 bonded carbon content and the enhanced hydrophobicity properties of the films.

1. Introduction

Glancing angle deposition (GAD) has emerged as a powerful tool to tailor the microstructure of the coatings deposited by physical vapor deposition, especially for the growth of the columnar crystal [1–4]. The shadow effect induced by the glancing incidence accounts for the formation of diverse three-dimensional microstructure, such as zigzags, nanopillar, nanorod, nanowire [2,4]. Till now, glancing angle deposition is adaptable to a wide variety of materials, including MgF_2 [5], ZnO [6], SiO_x [2,7], TiO_2 [1], $W_xSi_yO_z$ [8] and TiN-based thin films [9,10]. Very recently, the concept of GAD has also been introduced to the field of amorphous carbon film (a-C) [11–16], in order to tilt the nanoscale columnar structure [14], regulate the sp^3 content [15] and modify the hydrophobicity property of a-C film [16].

Tetrahedral amorphous carbon (ta-C) film, as one kind of a-C film with high sp^3 bonded carbon content and ultra-smooth surface, shows great potential as an outstanding protective coating in fields of ultra-high-density magnetic recording, MEMS devices, precision components [17,18]. The outstanding characteristics of ta-C film are tightly correlated with the high sp^3 content, which in return depend on the high deposition energy [19]. However, the carbon ions bombardment with high incident energy during deposition leads to the high residual compressive stress in the ta-C film, which endangers the excellent performance and serving lifetime. Effective methods have been attempted to reduce the residual stress of ta-C film, such as element doping, thermal annealing and bias applying, but this kind of stress reduction is at the substantial sacrifice of mechanical properties [20–23]. At present, the regulation of morphology, bond structure and residual stress of ta-C films by glancing angle deposition has been reported [12,13,24–26]. Xu et al. found that adjusting the incident angle of carbon ions resulted in a slight damage of hardness together with a significant reduction of residual stress [25]. In addition, the substrate tilting could alter the atomic bonds of ta-C films [26]. Taking the molecular dynamics simulation, the dependence of growth mode and surface morphology on GAD deposition of ta-C films were elucidated as well [27–30]. It could be said that the GAD technology can be a promising strategy to solve the current bottlenecks of ta-C films and endow it with other modified performance used in harsh environments, such as marine sliding components, precision glass molds for MEMS devices etc.

The electrochemistry dominated applications, such as biomolecules detection and corrosion protection has brought new opportunities for the development of ta-C film [31]. The modified physicochemical properties produced by GAD is expected to tailor the electrochemical

* Corresponding author at: Key Laboratory of Marine Materials and Related Technologies, Zhejiang Key Laboratory of Marine Materials and Protective Technologies, Ningbo Institute of Materials Technology and Engineering, Chinese Academy of Sciences, Ningbo 315201, China.
E-mail address: aywang@nimte.ac.cn (A. Wang).

https://doi.org/10.1016/j.apsusc.2020.146115
Received 22 October 2019; Received in revised form 14 February 2020; Accepted 16 March 2020
Available online 17 March 2020
0169-4332/

performance. Considering the lack of comprehensive knowledge on electrochemical behavior of ta-C films as a function of incident angle, we here fabricate the ta-C films by a home-made double bent FCVA system, where the macro-particles can be effectively filtered and the highly pure carbon ions are extracted to the substrate for the film deposition with high surface quality. The incident angle of carbon ions was varied from 0° to 75°, corresponding to the change of glancing angle during deposition. The structural evolution, mechanical properties and electrochemical behavior of ta-C films were focused as a function of the glancing angle.

2. Experimental procedures

2.1. GAD of ta-C films

Ta-C films were fabricated by a custom-made 45 degree double-bent filtered cathodic vacuum arc (FCVA) system whose details could be found in a previous publication [32]. Two kinds of p-type silicon (1 0 0) wafers were used as substrates, in which one with thickness of 280 ± 15 um was for accurate measurement of residual stress and another one of 545 ± 15 um was highly conductive silicon for microstructure characterization and electrochemical corrosion tests. Before deposition, the vacuum chamber was pumped to a base pressure of 2.0×10^{-5} Torr. Then, the substrates were subjected to Ar^+ plasma bombardment for 5 min to remove the surface contaminants. Subsequently, arc plasma was ignited by a mechanical striker and introduced to a double-bent filtering duct. The electromagnetic coils realized effective filtration of macro-particles and only high purity C^+ ions arrived at the substrates. The arc current and the duct voltage were set at 60 A and 20 V, respectively. Pulsed bias voltage of −50 V was applied to the substrate during all depositions. The glancing angle was defined as the angle between the incident C^+ stream and the normal direction of the substrate, as shown in Fig. 1. The glancing angle was varied from 0° to 75° (namely 0°, 15°, 30°, 45°, 60°, 75°). The film thickness was kept at 60 ± 5 nm by adjusting the deposition time for each glancing angle.

2.2. Characterization

The cross sections and surface morphologies of the films were obtained by field emission scanning electron microscope (FE-SEM, Thermo scientific Verios G4 UC, US). The film topographies in an area of 5 × 5 um^2 were acquired by atomic force microscope (AFM, Vecco Dimension 3100, US) operated in tapping mode. Raman spectrometer (Renishaw inVia-reflex, UK) was employed to analyze the chemical structure of the films with a wavelength of 532 nm and acquisition time of 30 s. The relative sp^3 content was determined by X-ray photoelectron spectroscopy (XPS, Axis ultradld, Japan) using monochromatic Al Kα source. The energy resolution of the XPS system was 0.6 eV. The binding energy was calibrated with C 1 s peak at 284.6 eV. Electron spin resonance spectrometer (ESR, Bruker E500, Germany) was employed to analyze the dangling bonds of the ta-C films. ESR spectra were recorded with X-band and 100 kHz field modulation at room temperature. The residual stress was calculated from the curvature of ta-C film coated Si (1 0 0) substrates according to the Stoney's equation, using a stylus profilometry (Alpha-Step IQ, US). Nano-indentation in the continuous stiffness measurement (CSM) mode was utilized to characterize the mechanical properties. OCA20 optical system (Dataphysics Ltd., Germany) was utilized to measure the static contact angle. The working liquids were 2 μl droplets of de-ionized water.

2.3. Electrochemical property

The electrochemical studies were carried out in 3.5 wt% NaCl solution using a Gamry Reference 600 potentiostat (US). A standard three-electrode system was set up for the measurement. The reference electrode was a KCl saturated silver/silver chloride (Ag/AgCl), the counter electrode was a platinum mesh and the working electrode was the tested specimen. The ta-C films on highly conductive silicon substrate were cut into 10 × 10 mm^2 square pieces and a conducting wire was stuck on the backsides of the cut samples using conductive silver glue. All exposed area except the working surface were sealed with epoxy resin. Each sample had a working surface of 1 cm^2. Prior to the tests, the whole system was soaked in 3.5 wt% NaCl solution for 1 h to stabilize the open circuit potential (OCP). Electrochemical impedance spectroscopy (EIS) was performed in the frequency from 100 kHz to 10 mHz. The applied sinusoidal perturbation was 10 mV. The EIS data were fitted and analyzed by the ZSimpWin software. Potentiodynamic polarization was carried out at 0.5 mV/s scanning rate from −0.6 V to +1.5 V vs. OCP.

3. Results and discussion

3.1. Deposition and morphology of the films

The typical amorphous structure of GAD deposited ta-C film was confirmed by HRTEM images (shown in Fig. S1). Fig. 2 shows the typical cross-sectional morphologies of ta-C films deposited at the glancing angle of 0°, 45° and 75°, respectively. For all the samples, a clear interface can be identified between the ta-C film and the silicon substrate. The film thickness were kept at 55 ± 5 nm when the glancing angle was changed from 0° to 75°. Moreover, noted that the films display the smooth surface without macro-droplets as other traditional

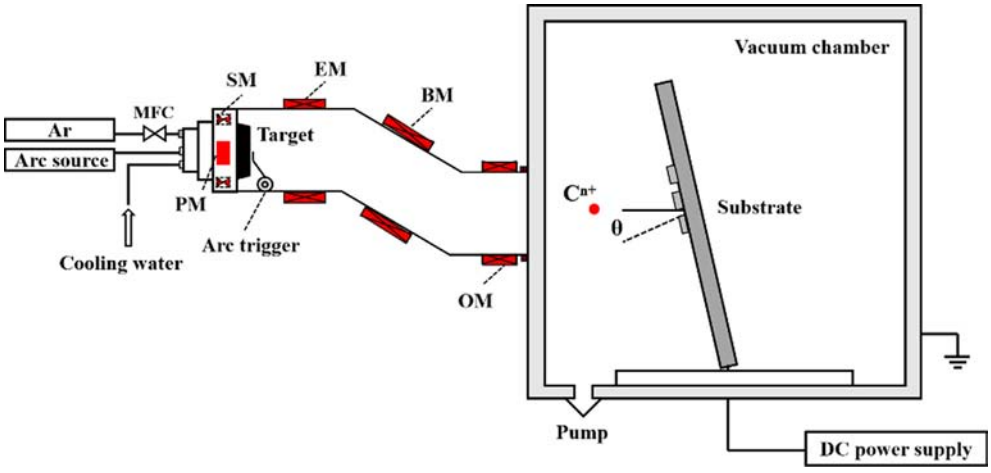

Fig. 1. Schematic diagram of glancing angle deposition.

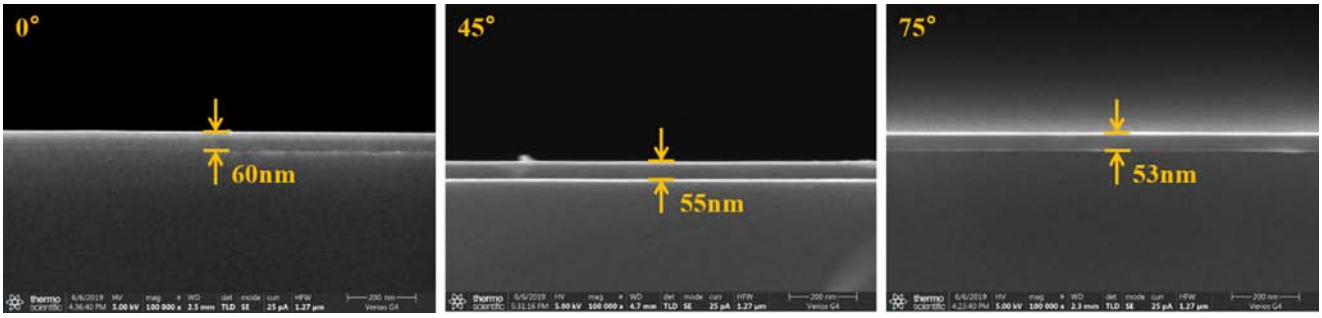

Fig. 2. Cross-sectional morphologies of ta-C films deposited at glancing angle of 0°, 45° and 75°.

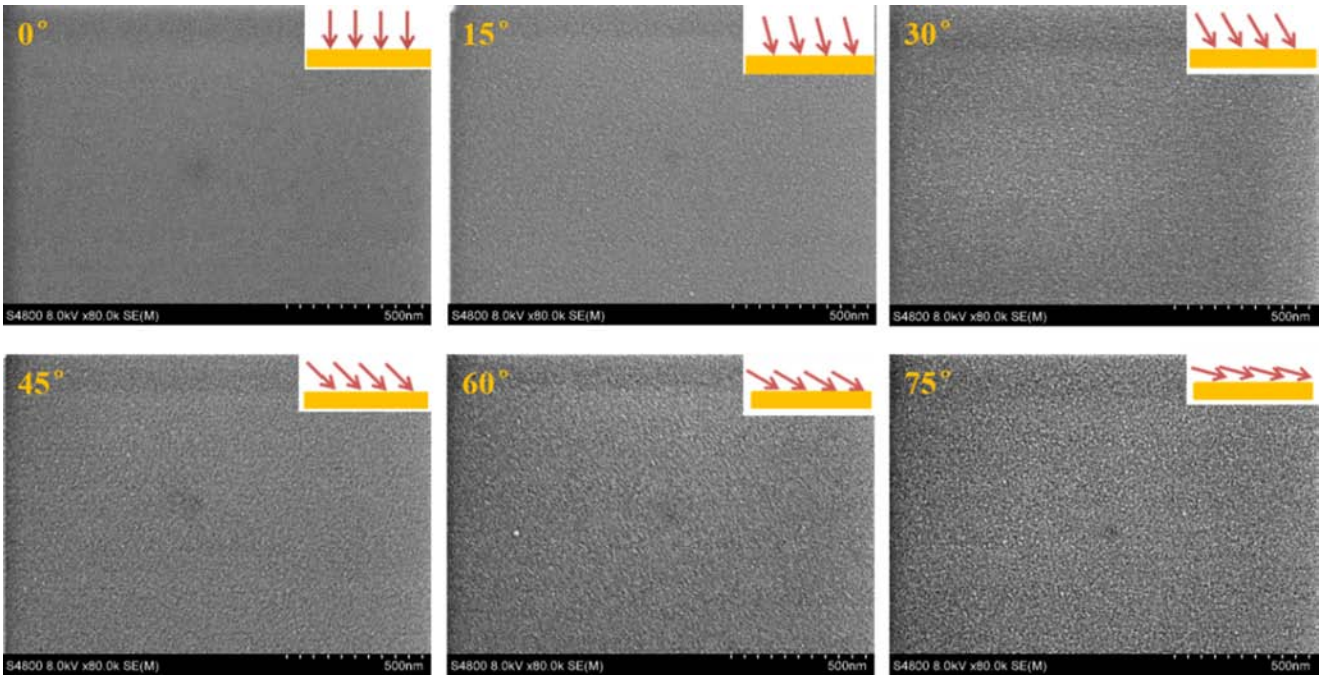

Fig. 3. Surface morphologies of the ta-C films deposited at various glancing angle.

cathode vacuum arc deposition.

Fig. 3 illustrates the surface morphologies of the ta-C films deposited at various glancing angles. The normal incident deposition of ta-C film ($\theta = 0°$) led to a smooth surface, while the introduction of glancing angle deposition produced some nano-texture on the film surface, in which nano-particles around 10 nm appeared. Meanwhile, the surface exhibited more agglomerated particles as the glancing angle increased from 15° to 75°, resulting in a rougher morphology. The absence of macro-particles in all top-morphology surface was consistent well with the above cross section results.

Fig. 4 presents the detailed topographic evolution in terms of root-mean-square roughness (R_a) and maximum roughness (R_{max}) deduced from AFM images (The AFM images with high resolution are shown in Fig. S2). The R_a increased from 0.38 to 0.47 nm with the increment of glancing angle from 0° to 15°, and then increased slightly as the glancing angle further increased to 60°. Finally, a relative sharp rise of surface roughness to 0.52 nm was proceeded when the glancing angle reached a value of 75°. The R_{max} showed a monotonous increase from 2.5 nm to 15.1 nm as the glancing angle varied from 0° to 75°. Therefore, it is rational to conclude that the variation of incident angle of carbon ions flux significantly altered the surface topology of the ta-C film.

In contrast to the normal incident deposition, the glancing incidence brings extra momentum parallel to the substrate, which significantly enhances the surface migration and diffusion, alter the growth kinetics. It was proposed by molecular dynamics (MD) simulation that the incident energy on the horizontal plane aggravated chaos and facilitated the surface roughening, while the incident energy on the vertical plane determined the voids defects and compactness of the film [27]. Different with the downhill transport of atoms induced surface smoothening at normal incidence, the uphill transport stemming from the significant lateral movement of the atoms at a grazing incidence resulted in the shadowing effect and rough surface [28].

3.2. Microstructure and composition of films

Atomic bond structure of the films was characterized by visible Raman and Fig. 5(a) shows the Raman spectra for clarity. All the spectra consist of two main peaks, one peak around 900–1000 cm^{-1} and the other broad peak around 1200–1800 cm^{-1}, which corresponds to the second-order signals of the silicon substrate due to the high transparence of ta-C film and the typical feature of amorphous carbon, respectively. After Gaussian fitting, the spectra can be decomposed to D peak and G peak, where D peak centered at 1360 cm^{-1} is originated from breath mode of sp^2 bonds and the G peak centered at 1560 cm^{-1} is due to the vibration mode of sp^2 bonds in both rings and chains. The area ratio of D peak and G peak was defined as I_D/I_G value. Fig. 5(b) shows the obtained I_D/I_G value and the G peak position as a function of incident angle. When the incident angle varied from 0° to 75°, the I_D/I_G value gradually increased and the G peak shifted downward to lower

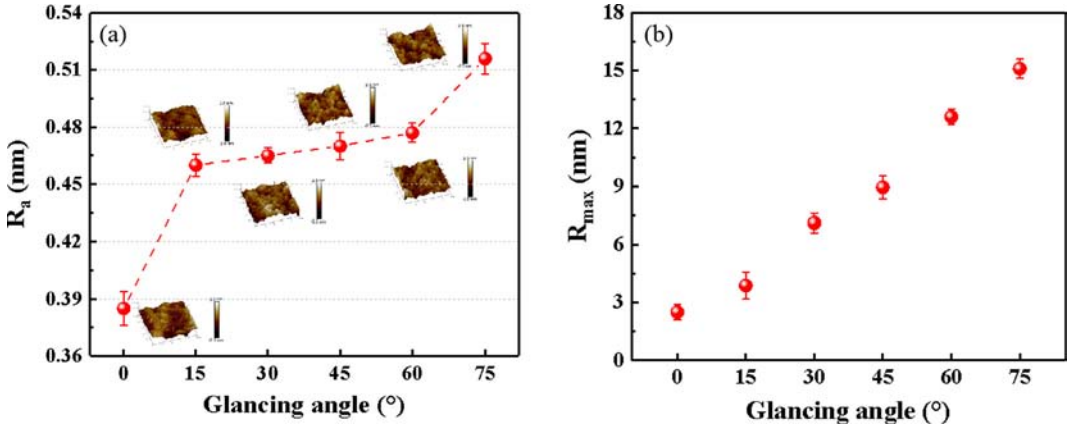

Fig. 4. (a) R_a (Insets are corresponding AFM images) and (b) R_{max} of ta-C films deposited at various glancing angle.

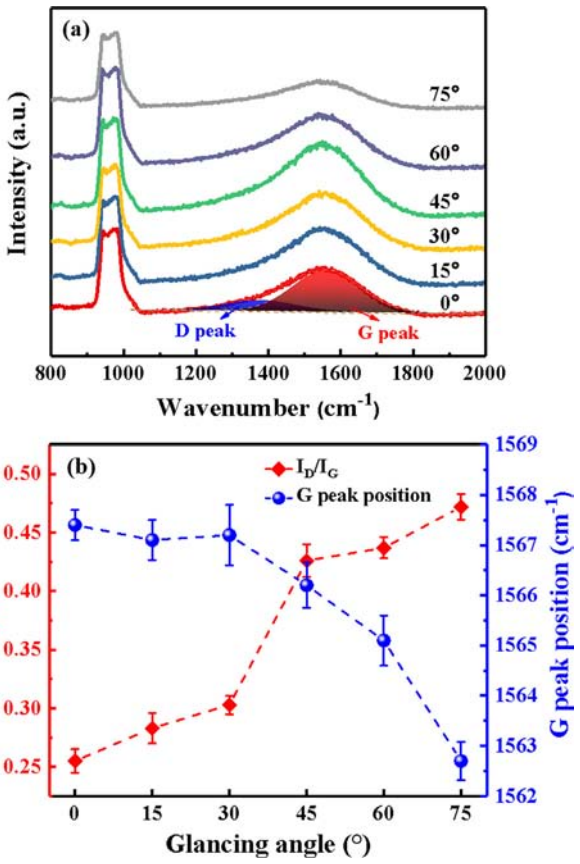

Fig. 5. (a) Raman spectra, (b) I_D/I_G ratio and G peak position of the ta-C films deposited at different glancing angles.

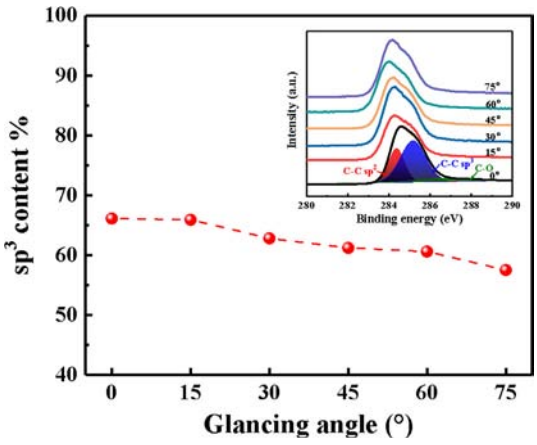

Fig. 6. The sp^3 contents of the ta-C films at different glancing angle. The inset show XPS C1s core level spectra as a function of glancing angle.

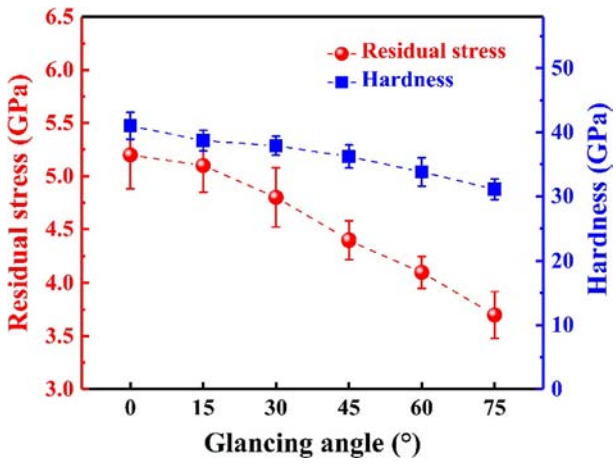

Fig. 7. The residual stress and hardness of the ta-C films as a function of glancing angle.

position, indicating the enhanced sp^2 phases and bond order [33,34]. Therefore, the number and size of the sp^2 cluster in the carbon network could experience a rise with the increase of incident angle, revealing the decreased sp^3 content.

Fig. 6 shows the XPS C1s core level spectra and the fitted results of the ta-C film deposited at various glancing angles. In order to investigate the hybridization states of carbon atoms, the spectra were fitted with three Gaussian peaks at 284.4 eV, 285.2 eV and 286.6 eV, corresponding to sp^2-C, sp^3-C and C-O, respectively [35]. The relative content of sp^3 bonded carbon atoms was calculated from the peak area ratio. When the incident angle increased from 0° to 75°, the sp^3 bonded carbon content decreased monotonously from 66 at.% to 57 at.%, which was attributed to the diminished momentum vertical to the substrate. As a consequence, increasing the glancing angle promoted the increase of sp^2 hybridized carbon atoms in the films [11,26].

3.3. Physicochemical properties of the films

Fig. 7 shows the evolution of the residual stress and hardness of the ta-C films as a function of glancing angle. The normal incidence ($\theta = 0°$) resulted in the highest compressive stress of 5.2 GPa due to the intensive impingement of high energetic carbon ions. The residual

stress exhibited a decreasing trend with increasing glancing angle from 0° to 75°. When the incident angle was 75°, the residual stress decreased to 3.7 GPa, revealing a reduction of 28.8% compared to that of 0°. This phenomenon could be attributed to several factors. XPS results demonstrated a 13.6% reduction of the sp^3 hybridized carbon atoms, which weakened the crosslink of the carbon network. On the other hand, the glancing angle deposition altered the growth kinetics of ta-C films. The structure relaxation of local distorted C-sp^3 bond lengths and bond angles could account for the stress reduction [25]. Furthermore, the shadow effect induced by oblique incidence could cause the island growth mode and rough surface. The trade-off between tensile stress stemmed from the coalescence of the islands and compressive stress owing to surface capillary forces of the island surfaces could determine the stress state of the films [11].

As shown in Fig. 7, the hardness decreased monotonously with the increase of incident angle of carbon ions. As the glancing angle varied from 0° to 75°, the hardness of the ta-C film evolved from 41.0 GPa to 31.1 GPa. The drop in hardness induced by glancing angle deposition was supposed to be originated from the reduction of sp^3 bonded carbon content [36]. Nevertheless, note that the ta-C film with low residual stress still maintained a relatively high hardness.

Electron spin resonance (ESR) is a powerful tool for evaluating the dangling-bond sites formed in amorphous carbon films. Fig. 8 shows the ESR results, where the bare silicon substrate exhibited faint signal, indicating the observed spectra were attributed to the ta-C films. All spectra of the films were featured by an isotropic broad single line and g factor of 2.0000. The effective spin density in the film were qualitatively analyzed by double integrating the ESR signal. As shown in Fig. 8(b), the spin density experienced a rapid rise as the glancing angle increased from 0° to 30°, and then tended to decrease with further increasing the glancing angle. The minimum spin density was obtained by glancing angle of 75°. An explanation for this phenomenon is that the spin density is the trade-off between several factors. When the glancing angle varied from 0° to 30°, the island growth mode led to a rougher surface, which enhanced the proportion of surface atoms in the film and thus produced more carbon atoms with unpaired electrons. Beyond 30°, the situation could be dominated by the reduction of sp^3 hybridized carbon atom along with the relaxation of distorted bond lengths and bond angles, which diminished the source of defect structure.

Wettability is an important parameter reflecting the surface property, which mainly depends on chemical composition, roughness and surface chemical bonds [37]. Contact angles of the ta-C films at different glancing angle are showed in Fig. 9. The contact angle gradually increased with the rise of incident angle from 0° to 45°, and then a sharp decrease emerged at glancing angle of 60° and 75°. Overall, the large contact angle was obtained by glancing angle of 30° and 45°, which is 68° and 72°, respectively. The variation of surface chemistry and topographical microstructure could account for this phenomenon. The

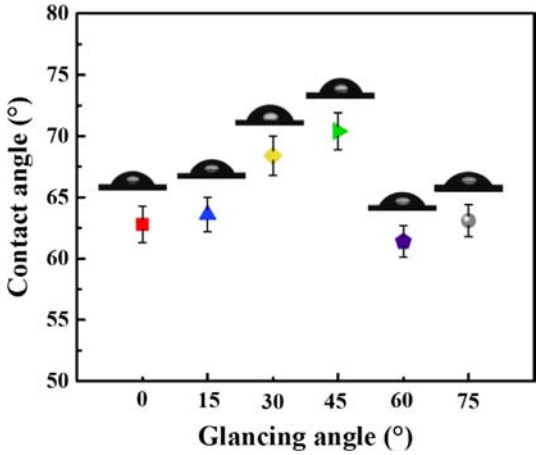

Fig. 9. Contact angle results of the ta-C films as a function of glancing angle.

dangling bonds influenced the surface free energy and contributed to a hydrophilic surface. However, the trend of spin density as a function of glancing angle was inconsistent with that of contact angle. In this regard, the surface geometric structure could be the predominant factor for the wettability. Despite the slight change of R_a, indicating the average surface roughness over 5 um × 5 um, the distinct increase of R_{max} revealed the significant changes between peak and valley over 5 um × 5 um. Particularly, R_{max} was about 7.11 nm and 8.71 nm for the glancing angle at 30° and 45°, in which the large contact angle was visible. It was reported that when the R_{max} of a surface with nanoparticles located in a specific range, a more hydrophobic surface was found in amorphous carbon films [38]. More importantly, the Wentzel equation and Cassie-Baxter equation could also be quoted to account for this phenomena [39]. When the glancing angle varied from 0° to 45°, a decrease of hydrophilicity was accompanied by an enhanced surface roughness, which belonged to Cassie-Baxter equation [40]. Thus, the rough surface would trap sufficient air in the grooves and hinder the penetration of the liquid into the low-lying area. Once the glancing angle reached 45°, the contact angle decreased with the increase of roughness, which was in accordance with the Wentzel equation [41]. According to the surface changes, it is speculated that the liquid spread into the rough grooves stimulates the transition from Cassie-Baxter equation to Wentzel equation at the critical glancing angle of 45°, due to the large surface area and surface energy stemmed from the sufficient coarseness. As a result, the tailored topology could induce the variation of contact angle.

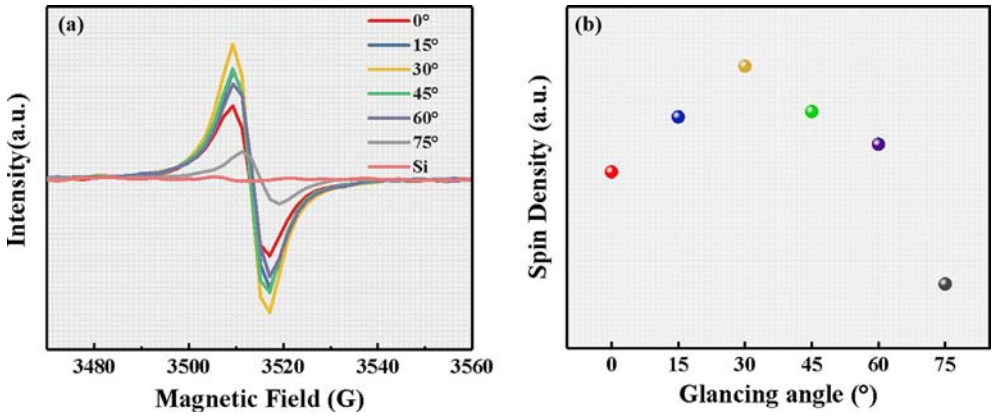

Fig. 8. (a) ESR spectra and (b) defects density of the ta-C films at different glancing angle.

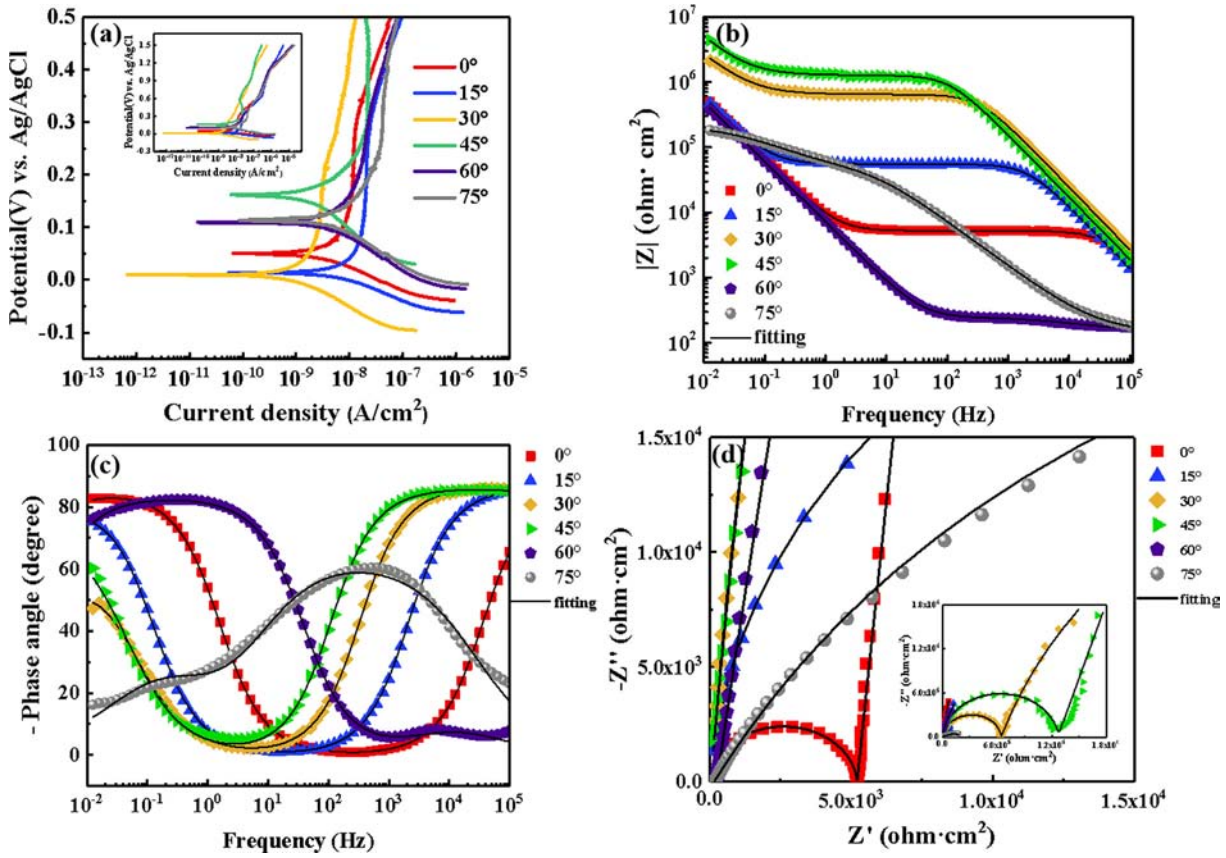

Fig. 10. (a) Potentiodynamic polarization curves, (b) Bode-modulus and (c) Bode-phase angle diagram, (d) Nyquist plots of the ta-C films deposited at different glancing angle (Inset shows the macrograph).

3.4. Electrochemical behaviors

Fig. 10 summaries the results of the electrochemical corrosion tests of the deposited ta-C films. According to the potentiodynamic polarization curves demonstrated in Fig. 10(a), the cathodic branches of all the samples showed similar features. Table 1 shows the electrochemical parameters deduced from the polarization curves through Tafel fitting. The ta-C films deposited at glancing angle of 30° and 45° presented lower anodic current densities of 3.56×10^{-10} A/cm^2 and 4.11×10^{-10} A/cm^2, respectively, indicating the weaker electrochemical activity. Moreover, the corrosion potential differed greatly, in which the film deposited at glancing angle of 45° has the highest value of 0.162 V, vs Ag/AgCl. Fig. 10(b) and (c) shows the corresponding Bode-modulus and Bode-phase angle diagram, respectively. At low and medium glancing angle of (0°-45°), the impedance modulus exhibited two different linear regions at low and high frequencies, and similar high frequency impedance values were observed at 10^5 Hz. The phase angle plot revealed two capacitance-dominant regions: one at low frequencies (below 10^{-1} Hz) and another at high frequencies (about 10^4 Hz), which reflecting the electrochemical reaction occurred at the electrolyte/substrate interface through the defects and the information related to ta-C film, respectively. In the case of 60° incident angle, a linear region of impedance modulus and a capacitive dominated region of phase angle were observed in the middle and low frequency regions. For glancing angle of 75°, the maximum phase angle was around −60° in the frequency range from 10^2 Hz to 10^3 Hz, indicting poor capacitive behavior. In general, a higher low frequency impedance at 0.01 Hz ($|Z|_{0.01Hz}$) indicates better corrosion resistance. It could be noted that the incident angle of 30° and 45° resulted in the superior $|Z|_{0.01Hz}$ value, followed by 0°, 15° and 60°, and 75° obtained the minimum value. The Nyquist plots in Fig. 10(d) demonstrated that ta-C films deposited at glancing angle of 45° obtained the largest arc radius, while the incident angle of 75° led to the smallest dimension of semi-circle loop.

The equivalent circuit (EC) was proposed to fit the EIS data and to gain insight into the electrochemical response of the testing system. Constant phase element (CPE) was employed to simulate the non-ideal capacitance behavior. As shown in Fig. 11, R_s represents the solution resistance, R_1 and R_2 correspond to pore resistance and charge transfer resistance, respectively. Q_1 and Q_2 is related to the constant phase element of the ta-C film and double layer capacitance, respectively. Similar equivalent circuit was widely employed to simulate the electrochemical corrosive behavior of the a-C coated system [42,43]. Table 2 summarized the fitting parameters of EIS data deduced from the equivalent circuit. The chi-square value (χ^2) was used to evaluate the fitting quality. Generally, a χ^2 value less than 10^{-2} indicates that the employed EC properly reflects the electrochemical corrosion behavior of the reaction system. From Table 1, all the χ^2 values were less than 2×10^{-3}, revealing good fitting qualities. This result was also

Table 1
Tafel fitting parameters of potentiodynamic polarization curves.

	0°	15°	30°	45°	60°	75°
Ecorr (V, vs Ag/AgCl)	0.049	0.013	0.012	0.162	0.110	0.114
I_{corr} (A/cm^2)	7.39×10^{-10}	1.30×10^{-9}	3.56×10^{-10}	4.11×10^{-10}	8.83×10^{-10}	1.05×10^{-9}

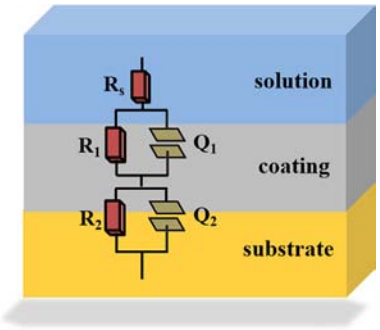

Fig. 11. The equivalent circuit for fitting EIS data.

supported by the coincidence of the fitting curve and the experimental data in Fig. 10(b)–(d). The polarization resistance R_p, a combination of R_1 and R_2, is an indicator of corrosion resistance. As a whole, the film deposited at glancing angle of 0°, 15° and 30° showed similar R_p value around $1.20 \times 10^7\ \Omega\ cm^{-2}$, and the film deposited at 45° incident angle obtained the highest R_p value of $8.95 \times 10^7\ \Omega\ cm^{-2}$. For the film deposited at glancing angle of 60° and 75°, the R_p value was $2.74 \times 10^6\ \Omega\ cm^{-2}$ and $2.20 \times 10^5\ \Omega\ cm^{-2}$, respectively. The n value reveals the deviation of the impedance from an ideal capacitor. For glancing angle of 75°, the n value for the constant phase element Q_1 and Q_2 was 0.61 and 0.73, indicating poor capacitive characteristic.

The factors determining the electrochemical corrosion behavior of ta-C film mainly include surface roughness, microstructure, electrical conductivity, residual stress and hydrophobicity [44–48]. The surface roughness correlates to the surface area exposed to the aggressive electrolyte, in which a rough surface provides more active sites to trigger electrochemical corrosion reaction [44]. The roughened surface and monotonously increased R_a and R_{max} as a function of glancing angle (Figs. 3 and 4) could deteriorate the corrosion resistance. More importantly, the electrical properties needs to be considered. It is the electron transport rather than the electron transfer that determines the electrochemical properties of ta-C film, due to the identical sp^2-rich surface layer [49]. In principal, the electron transport through the ta-C film is dominated by the sp^2 bonded carbon, which in return depend on the amount and size of the sp^2 cluster in the carbon network. The enhancement of sp^2 cluster contributes to form transportation channel for electrons and thus aggravates the electrochemical corrosion reaction. Therefore, the enhancement of sp^2 cluster (Fig. 5) and the promotion of sp^2/sp^3 ratio (Fig. 6) with the rise of glancing angle could narrow the mobility gap and facilitate the electron transportation through the ta-C film, thus accelerating the electrochemical reaction kinetics [46]. The stability of sp^3 hybrid carbon atom is superior to that of sp^2 bonded carbon atom, which indicated that the decreased sp^3 content (Fig. 6) degraded the anti-corrosion property [36]. By contrast, the reduction of residual stress (Fig. 7) was supposed to improve the anti-corrosion property [47]. Meanwhile, the surface reactivity of amorphous carbon plays a crucial role in electrochemical properties [50]. A large contact angle reflects low surface energy and weak adsorption effect of

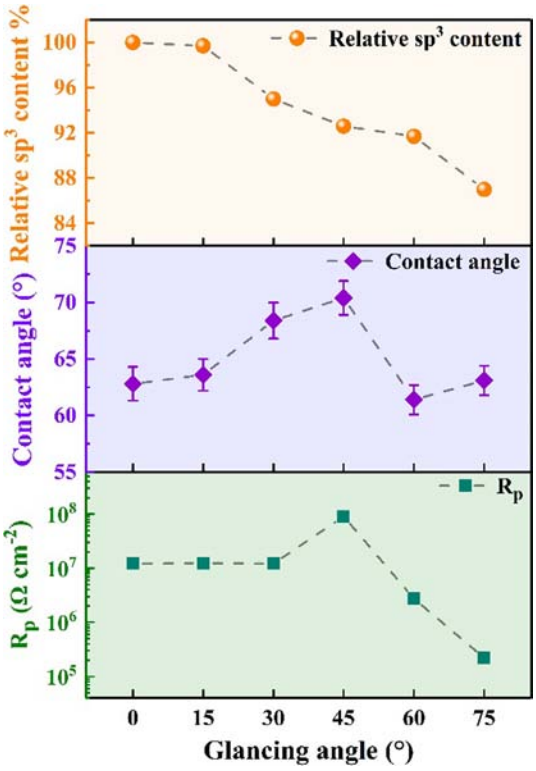

Fig. 12. Schematic showing the relationship between the physicochemical properties and the electrochemical corrosion resistance.

corrosive medium. Thus the evolution of contact angle contributed to regulate the corrosion behavior [48]. As shown in Fig. 12, the relationship between the physicochemical properties and the electrochemical corrosion resistance was summarized. The superimposition of the sp^3 content loss and the rise of contact angle resulted in the initial stable R_p value. Then the largest contact angle corresponded to the highest R_p. After that, the decrease of sp^3 content and a sharp drop in contact angle associated with more than one order of magnitude reduction in R_p value.

Accordingly, the schematic diagram of the electrochemical corrosion mechanism is presented in Fig. 13. In the case of nearly normal incident deposition (0°, 15°), ta-C film exhibited great corrosion resistance with polarization resistance over $10^7\ \Omega\ cm^{-2}$, due to high sp^3 bonded carbon content (66%) and smooth surface. At a higher deposition angle (30°, 45°), the ta-C film maintained relatively high sp^3 content (62%) and low surface roughness. Meanwhile, large contact angles were obtained, which diminished the reaction between the film and corrosive species and thus contributed to the improved anti-corrosion performance. When the incident angle further increased (60°, 75°), the reduced sp^3 content as well as the enhanced electrical conductivity deteriorated the corrosion resistance. Furthermore, the ta-C

Table 2
Fitted parameters obtained from EIS spectrum using the equivalent circuits.

	0°	15°	30°	45°	60°	75°
$R_s\ (\Omega\ cm^{-2})$	3.39	1.01	30.99	25.08	156.90	141.90
$Y_1\ (\Omega^{-2}\ cm^{-2}\ S^{-n})$	2.19×10^{-5}	1.97×10^{-9}	3.81×10^{-6}	1.51×10^{-9}	8.32×10^{-6}	1.14×10^{-5}
n_1	0.95	0.96	0.81	0.96	0.66	0.61
$R_1\ (\Omega\ cm^{-2})$	1.22×10^7	5.50×10^4	1.16×10^7	1.26×10^6	86.16	1.78×10^5
$Y_2\ (\Omega^{-2}\ cm^{-2}\ S^{-n})$	1.49×10^{-9}	2.27×10^{-5}	9.74×10^{-10}	2.13×10^{-6}	2.56×10^{-5}	1.54×10^{-6}
n_2	0.95	0.93	0.96	0.82	0.92	0.73
$R_2\ (\Omega\ cm^{-2})$	5.20×10^3	1.23×10^7	6.43×10^5	8.95×10^7	2.74×10^6	4.23×10^4
χ^2	4.35×10^{-5}	1.02×10^{-4}	4.19×10^{-4}	1.04×10^{-3}	4.03×10^{-4}	1.74×10^{-3}
$R_p\ (\Omega\ cm^{-2})$	1.22×10^7	1.24×10^7	1.22×10^7	9.08×10^7	2.74×10^6	2.20×10^5

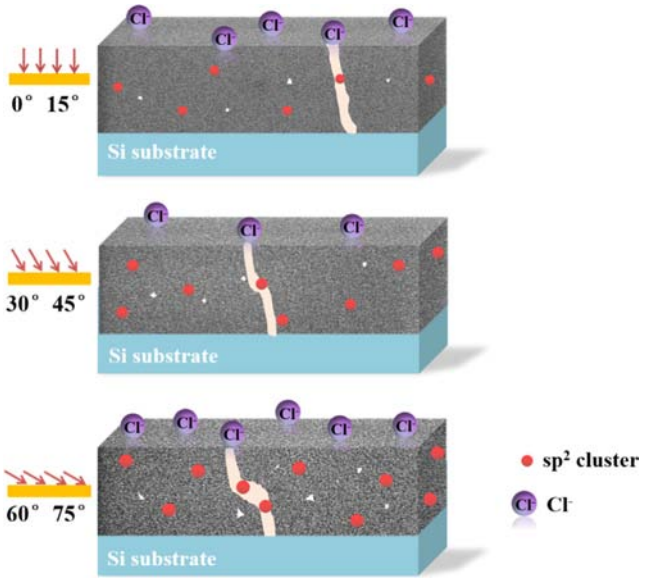

Fig. 13. The schematic diagram of the electrochemical corrosion mechanism of ta-C film deposited at various glancing angle.

film deposited at glancing angle of 75° owned the roughest surface which led to more exposed area to aggressive electrolyte, and the enhanced number and size of sp^2 clusters imbedded in the amorphous carbon network attenuated the resistance to transportation of electron.

4. Conclusions

A comprehensive study was conducted to study the effect of glancing angle on the structural evolution and electrochemical behavior of ta-C films. The results showed that the R_a rose from 0.38 nm to 0.52 nm and the surface exhibited more agglomerated particles as the glancing angle varied from 0° to 75°. It was worth noting that the residual stress exhibited a notable decline (28.8%) at the expense of a slight reduction (13.6%) of sp^3 hybridized carbon atoms. Despite the variation of incident angle, the hardness of ta-C films maintained a high value, exceeding 30 GPa. Moreover, the water contact angle and surface dangling bonds of ta-C film were found to be tailored by the incident angle of carbon ions.

Electrochemical corrosion results in 3.5 wt% NaCl solution showed that the ta-C film deposited at glancing angle of 45° possessed the superior corrosion resistance. The enhanced corrosion performance was attributed to the relatively high sp^3 hybrid carbon content and the enhanced hydrophobicity properties. In conclusion, the introduction of glancing angle deposition could endow ta-C film with novel microstructure and enhanced performance, which is of paramount importance for proceeding the exploration and application of ta-C film.

CRediT authorship contribution statement

Jing Wei: Conceptualization, Methodology, Data curation, Software, Writing - original draft, Writing - review & editing. **Peng Guo:** Writing - review & editing. **Linlin Liu:** Writing - review & editing. **Hanchao Li:** Data curation, Software. **Hao Li:** Data curation, Software. **Shuyuan Wang:** Data curation. **Peiling Ke:** Methodology, Supervision. **Aiying Wang:** Conceptualization, Methodology, Writing - review & editing, Supervision, Funding acquisition.

Declaration of Competing Interest

The authors declare that they have no known competing financial interests or personal relationships that could have appeared to influence the work reported in this paper.

Acknowledgements

The present research was funded by the National Science and Technology Major Project (2017-VII-0012-0108), A-class pilot of the Chinese Academy of Sciences (XDA22010303), Ningbo Science and Technology Innovation Project (2018B10014), Natural Science Foundation of Ningbo (2018A610175, 2018A610171). The authors also wish to thank Professor Hidetoshi Saito at Nagaoka University of Technology for helpful discussion.

Appendix A. Supplementary data

Supplementary data to this article can be found online at https://doi.org/10.1016/j.apsusc.2020.146115.

References

[1] H. Zhifeng, B. Fan, Wafer-scale, three-dimensional helical porous thin films deposited at a glancing angle, Nanoscale 6 (2014) 9401–9409.
[2] Y. Zhao, D. Ye, G.C. Wang, T.M. Lu, Designing nanostructures by glancing angle deposition, Proc. SPIE 5219 (2003) 59–73.
[3] M.M. Hawkeye, M.J. Brett, Glancing angle deposition: Fabrication, properties, and applications of micro- and nanostructured thin films, J. Vac. Sci. Technol., A 25 (2007) 1317–1335.
[4] A. Barranco, A. Borras, A.R. Gonzalez-Elipe, A. Palmero, Perspectives on oblique angle deposition of thin films: From fundamentals to devices, Prog. Mater. Sci. 76 (2016) 59–153.
[5] S. Bruynooghe, D. Tonova, M. Sundermann, T. Koch, U. Schulz, Antireflection coatings combining interference multilayers and a nanoporous MgF 2 top layer prepared by glancing angle deposition, Surf. Coat. Technol. 267 (2015) 40–44.
[6] S. Mukhtar, A. Asadov, W. Gao, Microstructure of ZnO thin films produced by magnetron sputter oblique deposition, Thin Solid Films 520 (2012) 3453–3457.
[7] S. Sarkar, S.K. Pradhan, Tailoring of optical and wetting properties of sputter deposited silica thin films by glancing angle deposition, Appl. Surf. Sci. 290 (2014) 509–513.
[8] J. Gilrostra, M. Cano, J.M. Pedrosa, F.J. Ferrer, F. Garcíagarcía, F. Yubero, A.R. Gonzálezelipe, Electrochromic Behavior of WxSiyOz Thin Films Prepared by Reactive Magnetron Sputtering at Normal and Glancing Angles, ACS Appl. Mater. Interfaces 4 (2011) 628.
[9] J. Zheng, Y. Lv, S. Xu, X. Han, S. Zhang, J. Hao, W. Liu, Nanostructured TiN-based thin films by a novel and facile synthetic route, Mater. Des. 113 (2017) 142–148.
[10] P. Pedrosa, D. Machado, P. Fiedler, B. Vasconcelos, E. Alves, N.P. Barradas, N. Martin, J. Haueisen, F. Vaz, C. Fonseca, Electrochemical characterization of nanostructured Ag:TiN thin films produced by glancing angle deposition on polyurethane substrates for bio-electrode applications, J. Electroanal. Chem. 768 (2016) 110–120.
[11] Y. Lei, J. Jiang, Y. Wang, T. Bi, L. Zhang, Structure evolution and stress transition in diamond-like carbon films by glancing angle deposition, Appl. Surf. Sci. 479 (2019) 12–19.
[12] FanXin Liu, KaiLun Yao, ZuLi Liu, Substrate bias effect on structure of tetrahedral amorphous carbon films by Raman spectroscopy, Diamond Relat. Mater. 16 (2007) 1746–1751.
[13] N. Wang, K. Komvopoulos, Incidence angle effect of energetic carbon ions on deposition rate, topography, and structure of ultrathin amorphous carbon films deposited by filtered cathodic vacuum Arc, IEEE Trans. Magn. 48 (2012) 2220–2227.
[14] M. Hirokatsu, K. Wataru, S. Akira, I. Yohei, N. Takashi, W. Masatoshi, B. Avi, P.J. Martin, Epitaxial-like growth of anisotropic mesostructure on an anisotropic surface of an oblique nanocolumnar structure, J. Am. Chem. Soc. 132 (2010) 9414–9419.
[15] J. Matlak, K. Komvopoulos, Ultrathin amorphous carbon films synthesized by filtered cathodic vacuum arc used as protective overcoats of heat-assisted magnetic recording heads, Sci. Rep. 8 (2018) 9647.
[16] R.Z. Moghadam, M.H. Ehsani, H.R. Dizaji, P. Kameli, M. Jannesari, Modification of hydrophobicity properties of diamond like carbon films using glancing angle deposition method, Mater. Lett. 220 (2018) 301–304.
[17] S.H. Kim, D.B. Asay, M.T. Dugger, Nanotribology and MEMS, Nano Today 2 (2007) 22–29.
[18] C. Casiraghi, J. Robertson, A.C. Ferrari, Diamond-like carbon for data and beer storage, Mater. Today 10 (2007) 44–53.
[19] M.A. Caro, V.L. Deringer, J. Koskinen, T. Laurila, G. Csányi, Growth mechanism and origin of high sp3 content in tetrahedral amorphous carbon, Phys. Rev. Lett. 120 (2018) 166101.
[20] A.Y. Wang, K.R. Lee, J.P. Ahn, J.H. Han, Structure and mechanical properties of W incorporated diamond-like carbon films prepared by a hybrid ion beam deposition technique, Carbon 44 (2006) 1826–1832.
[21] M. Constantinou, P. Nikolaou, L. Koutsokeras, A. Avgeropoulos, D. Moschovas, C. Varotsis, P. Patsalas, P. Kelires, G. Constantinides, Metal (Ag/Ti)-Containing Hydrogenated Amorphous Carbon Nanocomposite Films with Enhanced

Nanoscratch Resistance: Hybrid PECVD/PVD System and Microstructural Characteristics, Nanomaterials 8 (2018) 209.
[22] A.C. Ferrari, B. Kleinsorge, N.A. Morrison, A. Hart, V. Stolojan, J. Robertson, Stress reduction and bond stability during thermal annealing of tetrahedral amorphous carbon, J. Appl. Phys. 85 (1999) 7191–7197.
[23] H. Liang, D. Liu, C. Xian, Y. Li, Y. Zhao, The deposition of a thick tetrahedral amorphous carbon film by argon ion bombardment, Appl. Surf. Sci. 258 (2012) 4794–4800.
[24] J. Matlak, K. Komvopoulos, Ultrathin amorphous carbon films synthesized by filtered cathodic vacuum arc used as protective overcoats of heat-assisted magnetic recording heads, Sci. Rep. 8 (2018) 9647.
[25] S. Xu, X. Li, M. Huang, P. Ke, A. Wang, Stress reduction dependent on incident angles of carbon ions in ultrathin tetrahedral amorphous carbon films, Appl. Phys. Lett. 104 (2014) 141908.
[26] F.-X. Liu, K.-L. Yao, Z.-L. Liu, Substrate tilting effect on structure of tetrahedral amorphous carbon films by Raman spectroscopy, Surf. Coat. Technol. 201 (2007) 7235–7240.
[27] C. Xue, J. Zhou, An atomistic study of growth mode and microstructure evolution of amorphous carbon films by different incident carbon atoms, Appl. Surf. Sci. 314 (2014) 973–982.
[28] M. Joe, M.-W. Moon, J. Oh, K.-H. Lee, K.-R. Lee, Molecular dynamics simulation study of the growth of a rough amorphous carbon film by the grazing incidence of energetic carbon atoms, Carbon 50 (2012) 404–410.
[29] B. Schultrich, Modeling of ta-C growth: Influence of the technological parameters, Diamond Relat. Mater. 20 (2011) 785–792.
[30] X. Li, P. Ke, K.-R. Lee, A. Wang, Molecular dynamics simulation for the influence of incident angles of energetic carbon atoms on the structure and properties of diamond-like carbon films, Thin Solid Films 552 (2014) 136–140.
[31] T. Laurila, S. Sainio, M.A. Caro, Hybrid carbon based nanomaterials for electrochemical detection of biomolecules, Prog. Mater Sci. 88 (2017) 499–594.
[32] J. Wei, H. Li, L. Liu, P. Guo, P. Ke, A. Wang, Enhanced tribological and corrosion properties of multilayer ta-C films via alternating sp3 content, Surf. Coat. Technol. 374 (2019) 317–326.
[33] A.C. Ferrari, J. Robertson, Resonant Raman spectroscopy of disordered, amorphous, and diamondlike carbon, Phys. Rev. B: Condens. Matter Mater. Phys. 64 (2001) 075414.
[34] S. Prawer, K.W. Nugent, Y. Lifshitz, G.D. Lempert, E. Grossman, J. Kulik, I. Avigal, R. Kalish, Systematic variation of the Raman spectra of DLC films as a function of sp2:sp3 composition, Diamond Relat. Mater. 5 (1996) 433–438.
[35] B. Lesiak, L. Kövér, J. Tóth, J. Zemek, P. Jiricek, A. Kromka, N. Rangam, C sp2 /sp3 hybridisations in carbon nanomaterials – XPS and (X)AES study, Appl. Surf. Sci. 452 (2018) 223–231.
[36] J. Robertson, Diamond-like amorphous carbon, Mater. Sci. Eng., R 37 (2002) 129–281.
[37] B. Zhang, S. Lu, W. Xu, Y. Cheng, Controllable wettability and morphology of electrodeposited surfaces on zinc substrates, Appl. Surf. Sci. 360 (2016) 904–914.
[38] L. Sun, G. Peng, P. Ke, X. Li, A. Wang, Synergistic effect of Cu/Cr co-doping on the wettability and mechanical properties of diamond-like carbon films, Diamond Relat. Mater. 68 (2016) 1–9.
[39] C. Ishino, K. Okumura, D. Quéré, Wetting transitions on rough surfaces, Europhys. Lett. (EPL) 68 (2004) 419–425.
[40] A.B.D. Cassie, Contact angles, Discuss. Faraday Soc. 3 (1948).
[41] R.N. Wenzel, Resistance of solid surfaces to wetting by water, Ind. Eng. Chem. Res. 28 (1936) 988–994.
[42] L. Mohan, C. Anandan, V.K.W. Grips, Corrosion behavior of titanium alloy Beta-21S coated with diamond like carbon in Hank's solution, Appl. Surf. Sci. 258 (2012) 6331–6340.
[43] A. Zeng, Impedance study on electrochemical characteristics of sputtered DLC films, Thin Solid Films 426 (2003) 258–264.
[44] N.W. Khun, E. Liu, X.T. Zeng, Corrosion behavior of nitrogen doped diamond-like carbon thin films in NaCl solutions, Corros. Sci. 51 (2009) 2158–2164.
[45] A.S. Hamdy, Electrochemical behavior of diamond-like-carbon coatings deposited on AlTiC (AlO + TiC) ceramic composite substrate in HCl solution, Electrochim. Acta 56 (2011) 1554–1562.
[46] T. Palomäki, N. Wester, M.A. Caro, S. Sainio, V. Protopopova, J. Koskinen, T. Laurila, Electron transport determines the electrochemical properties of tetrahedral amorphous carbon (ta-C) thin films, Electrochim. Acta 225 (2017) 1–10.
[47] J. Choi, S. Nakao, J. Kim, M. Ikeyama, T. Kato, Corrosion protection of DLC coatings on magnesium alloy, Diamond Relat. Mater. 16 (2007) 1361–1364.
[48] Y. Zhuang, X. Jiang, A.V. Rogachev, D.G. Piliptsou, B. Ye, G. Liu, T. Zhou, A.S. Rudenkov, Influences of pulse frequency on the structure and anti-corrosion properties of the a-C: Cr films, Appl. Surf. Sci. 351 (2015) 1197–1203.
[49] T. PalomäKi, N. Wester, M.A. Caro, S. Sainio, V. Protopopova, J. Koskinen, T. Laurila, Electron transport determines the electrochemical properties of tetrahedral amorphous carbon (ta-C) thin films, Electrochim. Acta 225 (2017) 1–10.
[50] M.A. Caro, A. Aarva, V.L. Deringer, G. Csányi, T. Laurila, Reactivity of amorphous carbon surfaces: rationalizing the role of structural motifs in functionalization using machine learning, Chem. Mater. 30 (2018) 7446–7455.